Checking and Correcting DTI Data

7

Chantal M.W. Tax, Sjoerd B. Vos,
and Alexander Leemans

Learning Points

- Data quality assurance is important in DTI.
- Artifacts can severely affect subsequent qualitative and quantitative analyses.
- Bad data quality can be detected during acquisition or image processing.
- Correction of artifacts can be done during the acquisition and image processing stage.
- Quality assurance can be used to improve data quality on the scanner.

Introduction

Diffusion MRI data is, like any other MRI technique, prone to artifacts. Most diffusion MRI analyses are based on a voxel-wise computation of quantities from a series of diffusion-weighted images (DWIs) acquired with different orientation and magnitude of diffusion sensitization, and the results may be severely affected by artifacts. It is therefore of great importance to avoid or correct for these artifacts before subsequent analyses [1].

There are various ways to classify artifacts in diffusion MRI data. They may be present in the DWIs themselves (e.g., Gibbs ringing, susceptibility artifacts), or become apparent when combining all DWIs (e.g., subject motion). Some artifacts are related to MRI acquisition in general (e.g., Gibbs ringing and EPI distortions) or are specific to diffusion weighting. Spin-echo echo-planar imaging (SE EPI) is often the method of choice for diffusion acquisition since it is a relatively fast technique, but the resulting images are locally distorted due to differences in tissue susceptibility. The rapid switching of gradients required when acquiring diffusion MRI data leads to eddy current distortions. The origin of some artifacts is system related (e.g., eddy current distortions, signal dropouts, vibration artifacts), whereas others are subject related (subject motion, susceptibility artifacts).

In this chapter, we will review the most clinically relevant artifacts from different angles. It is not the purpose to extensively discuss each artifact, but to focus on the practical issues instead. The origin, recognition, and correction methods for each artifact are briefly outlined in the first section, where we specifically focus on the different processing stages (Fig. 7.1). We will distinguish

C.M.W. Tax, MSc (✉) • A. Leemans, PhD
PROVIDI Lab, Image Sciences Institute, University Medical Center Utrecht, Room E.02.5.54, 3508 GA Utrecht, The Netherlands
e-mail: chantal@isi.uu.nl

S.B. Vos, PhD
PROVIDI Lab, Image Sciences Institute, University Medical Center Utrecht, Room E.02.5.54, 3508 GA Utrecht, The Netherlands

Translational Imaging Group, Centre for Medical Image Computing, University College London (UCL), London, UK

W. Van Hecke et al. (eds.), *Diffusion Tensor Imaging*, DOI 10.1007/978-1-4939-3118-7_7

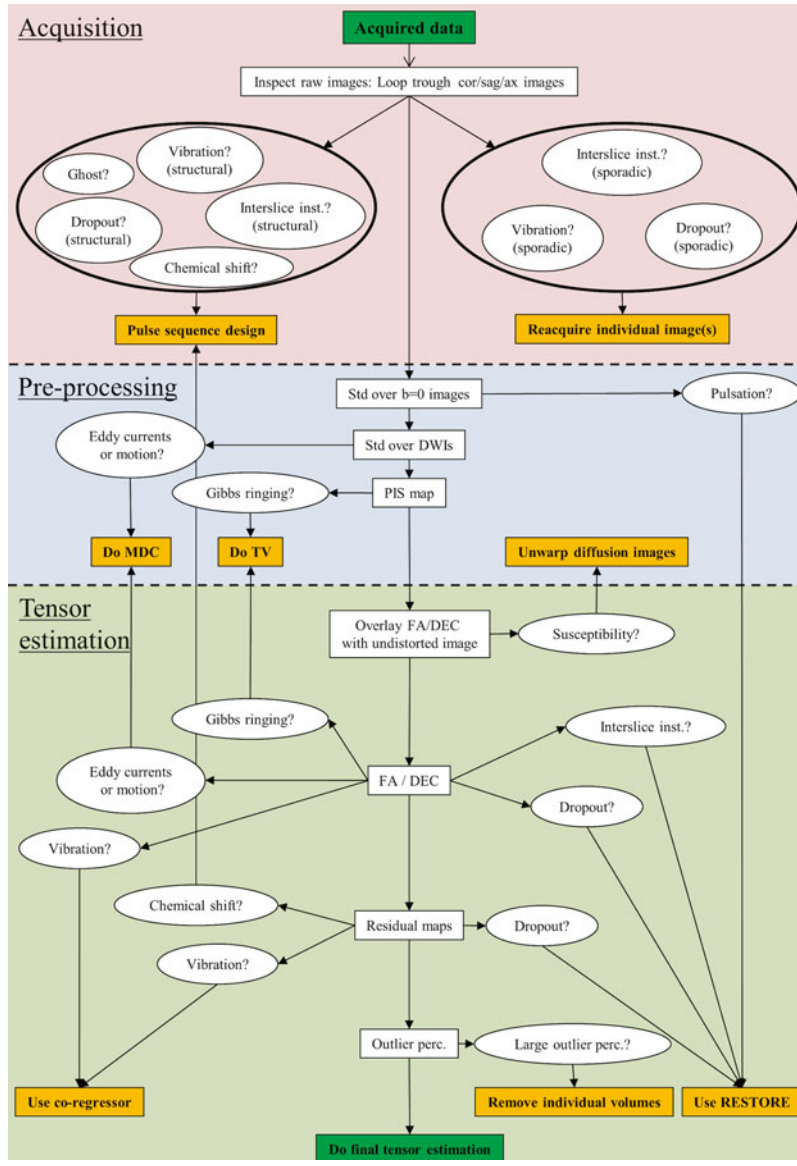

Fig. 7.1 Decision tree scheme for checking and correcting of diffusion data. *Std standard deviation*, *interslice inst.* interslice instabilities, *PIS* physically implausible signal, *MDC* motion-distortion correction, *TV* total variation, *FA*/*DEC* direction-encoded FA map, *perc.* percentage

the acquisition stage, in which we consider recognition and correction on raw data only, from the image processing stage, which includes any form of processing of the data (e.g., fitting a tensor or calculating standard deviations of the measurements). The central question throughout this chapter is: *How can I recognize and, potentially, correct for artifacts, either during scanning or when I have already acquired the data*? We present a decision tree scheme, which can be used as a stepwise manual for optimal data acquisition and processing (including pre-processing and tensor estimation), answering the question to *which acquisition and processing methods to consider in a stepwise manner for optimal data quality for subsequent analysis*? Obviously, prevention is better than cure, which is why we will discuss methods to assure data quality in the second section. Quality assurance (QA) focuses on *how to make sure that the scanner is able to acquire high quality data, before actual patient data acquisition*. We provide some examples when to accept or reject data. Finally, it is important to understand *how artifacts influence quantitative and directional diffusion MRI mea-*

sures. To this end, the last section focuses on the possible effect of artifacts on voxel-wise computed quantitative measures such as mean diffusivity (MD) and fractional anisotropy (FA) and on tractography results. The guidelines for checking and correcting data presented in this chapter are not specific to DTI only, but often extend to other diffusion acquisition techniques such as high angular resolution diffusion imaging (HARDI).

Recognition and Correction of Artifacts

Eddy Current-Induced Distortions

Origin

Conductive elements of the MRI scanner (e.g., the gradient coils) permit the flow of electric charges. When a conductor is located in a changing magnetic field, this will induce currents in the conductor. Because their flow patterns resemble swirling eddies in a river, they are called eddy currents. Besides gradients for spatial localization of the MR signal, additional magnetic gradients are used to make MR sensitive to diffusion. The diffusion-sensitizing gradients have to be switched on and off very rapidly, and induce eddy currents [2] in conductors present. The eddy currents, in turn, induce additional magnetic gradient fields which will change the actual diffusion gradient, as can be seen in Fig. 7.2b, where the actual diffusion gradient is different from the desired one in Fig. 7.2a. The effect on the DWIs is twofold: overlap of the changed diffusion gradient with spatial encoding gradients will lead to geometric distortions and thus misalignment of individual DWIs; and the deviation of the diffusion gradient from what we expect will lead to errors in diffusion estimates.

Recognition and Correction in Acquisition Stage

When eddy current-induced fields overlap with the spatial encoding period of the image acquisition, this will lead to geometric distortions. These distortions are visible in the raw DWIs in the phase-encoding direction (PE, most commonly anterior–posterior or y-direction) and depend on the direction of the eddy current gradient. An eddy current gradient in left–right (x) direction will result in a shear in the axial (xy) plane, assuming that the PE direction is anterior–posterior (y). Likewise, an eddy current gradient in y-direction causes scaling in y-direction (Fig. 7.3a shows compression in y-direction), whereas eddy current gradients in inferior–superior (z) direction translates each slice in y-direction dependent on the slice position [3].

Generation of eddy currents is inevitable in diffusion MRI; however, there are methods to minimize them. Replacing the single-refocused spin-echo diffusion preparation (Fig. 7.2a) by a twice-refocused spin-echo (TRSE) preparation (Fig. 7.2c) reduces the eddy currents resulting in less severe geometric distortions [4]. This is also

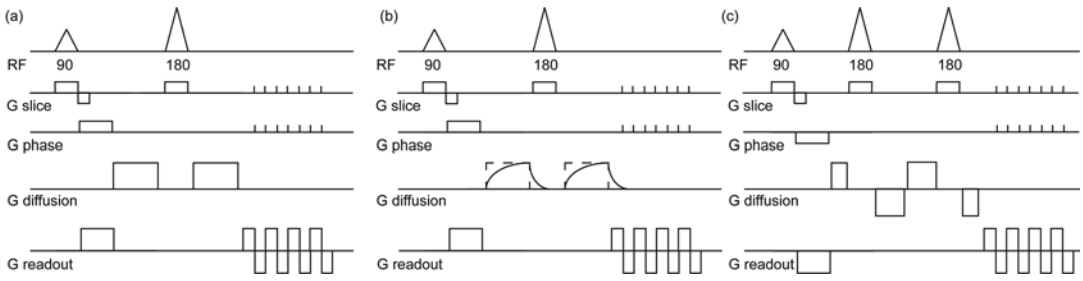

Fig. 7.2 Diffusion MR sequences. (**a**) For the standard, once-refocused, diffusion preparation, after the excitation (90° RF pulse) there are two gradients that sensitize the signal to diffusion, with a refocusing pulse (180° radio-frequency (RF) pulse) at half the echo time (TE/2) to form an echo during the readout. (**b**) The diffusion gradient is not as desired and overlaps with the spatial encoding gradients. (**c**) TRSE: The twice-refocused diffusion preparation (*bottom line*) has two refocusing pulses splitting four gradient blocks to form an echo during the readout

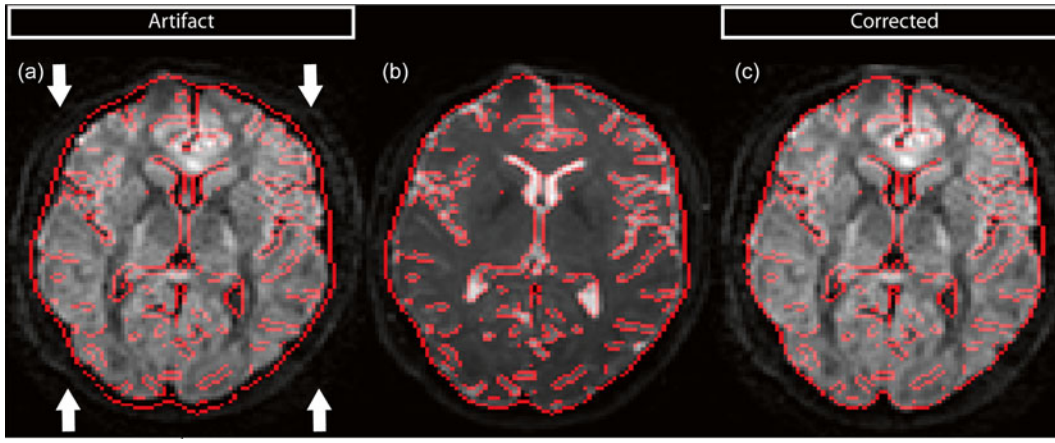

Fig. 7.3 Example of DW image with scaling induced by eddy currents in the phase-encoded anterior–posterior (AP, indicated by the *arrows*) direction (**a**), compared to the undistorted B_0 image (**b**). The lines overlaid in red indicate brain edges and boundaries of the undistorted B_0 image. (**c**) Raw data in which the effect of eddy currents is minimized

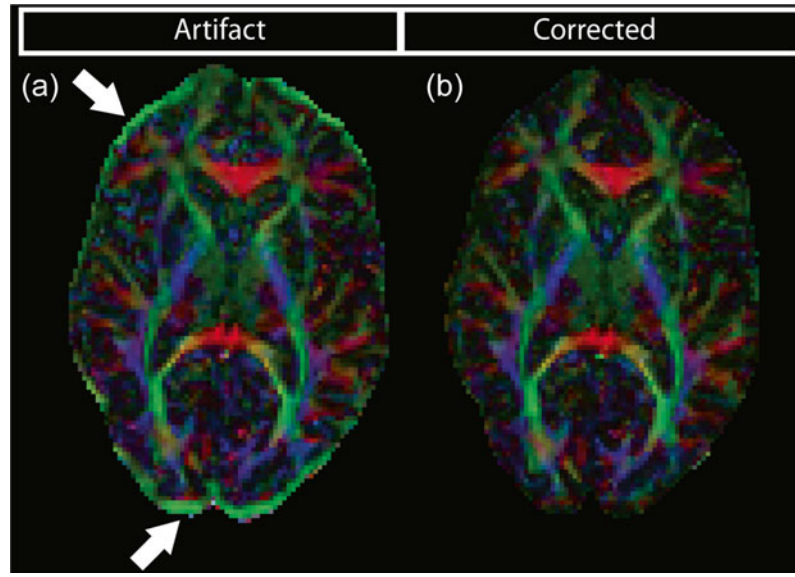

Fig. 7.4 (**a**) DEC map showing an orientational bias in the high anisotropy rim at the periphery of the brain. (**b**) The same map calculated after distortion correction

called dual spin-echo (DSE) diffusion imaging. The TRSE/DSE diffusion sequence is available in most, if not all, recent MRI scanners, making this an easy to use option. Figure 7.3c shows a raw image with minimal eddy current distortions. The downside of a TRSE sequence is a small increase in echo time (TE), caused mainly by the additional 180 pulse. As a result, the signal-to-noise ratio (SNR) decreases and the repetition time (TR) may increase, which would result in a longer acquisition time.

Recognition and Correction in Image Processing Stage

Different geometric distortions of every individual DWI will result in misalignment of the images, which will, in general, affect diffusion-derived measures that are estimated on a voxel-by-voxel basis. Eddy current-induced misalignment artifacts become visible as bands of increased FA at the periphery of the brain (Fig. 7.4a) but, although less pronounced, are also present throughout the brain. The direction-

encoded color (DEC) maps [5] furthermore show a dominant orientation in these bright rims, which is typical for eddy current-induced geometric distortions when they are only visible in the phase-encoding (PE) orientation of the image.

Correction for eddy current-induced distortions is commonly done in the diffusion MRI image processing pipeline. Various image registration based methods have been developed for correction [2, 6, 7]. Typically, mutual information is used to register all DWIs to the non-DW ($b=0$) image, which has no eddy current-induced distortions. For this purpose no additional scans are needed. Figure 7.4b displays the DEC map after correction.

Besides image distortions, eddy currents can also influence diffusion measurements in another way. Figure 7.2b already showed that the actually applied diffusion gradient differs from the desired one. The diffusion weighting of an image is thus not exactly what we expect, which will result in errors in the estimates of the diffusion parameters. This is often hard to recognize and impractical to correct for.

Subject Motion

Origin

The acquisition of a typical clinical DTI dataset takes around 5–10 min, for research purposes this can even be longer. Although subjects are instructed to lie still during a scan, head or body motion is difficult to avoid. Motion can be subdivided into translations (in *x*-, *y*-, and *z*-direction) and rotations (yaw, pitch, and roll). Many DWIs have to be acquired to estimate diffusion properties accurately, and misalignment due to motion will lead to errors in these estimates.

Recognition and Correction in Acquisition Stage

Instead of a time-consuming detailed slice-by-slice inspection of the raw DW MRI data, subject motion can also be investigated by looping through the DW images at a frame rate of approximately ten frames per second, or quickly toggling between the first and last acquired DW MRI image.

During acquisition, all care should be taken to immobilize the subject. This is commonly done by placing cushions, or pads, between the subject's head and the inside of the head coil. This makes it easier for the subject to keep his or her head still.

Even for the most willing and cooperative subjects, head motion is likely to occur to some extent. Slight movement of the brain may result in a mismatch between subsequent slices, which means these slices cannot be combined correctly. Several new pulse sequences have been proposed that can correct for *in-plane* motion, e.g., PROPELLER or SNAILS [8]. However, these cannot correct for *through-plane* motion. Prospective volume registration can account for through-plane motion. Here, the field-of-view (FOV) is repositioned after each 3D image volume, so after each TR. This method can correct the motion for any subsequent volume accurately, but the volume in which motion occurred is corrupt and must be re-acquired, elongating the scan time. To truly account for any motion, however, the motion must be detected with a higher temporal resolution. Zaitsev et al. [9] proposed such a real-time prospective motion correction setup: when head motion is detected, the imaging field-of-view is adjusted accordingly for the next excitation. Their system used a mouthpiece with markers outside the mouth that could be imaged by optical cameras outside of the magnet bore. In this way, rigid body motion of the head can be detected and corrected for a wide range of rotations and translations. Recent advances in this field were focused on ease-of-use as well as correction accuracy, with methods that use a small object attached to the subject's forehead that is imaged by a camera within the bore, capable of correcting translations and rotations as small as 10 μm and 0.01° [10, 11]. For an extensive overview, one is referred to [12]. Currently, these methods are transforming from a purely developmental setup to products shared between neuroscientific research groups.

Recognition and Correction in Image Processing Stage

Subject motion will, just like eddy current geometric distortions, result in misregistration of DW volumes. This misregistration can in some cases also be recognized by rims of high anisotropy

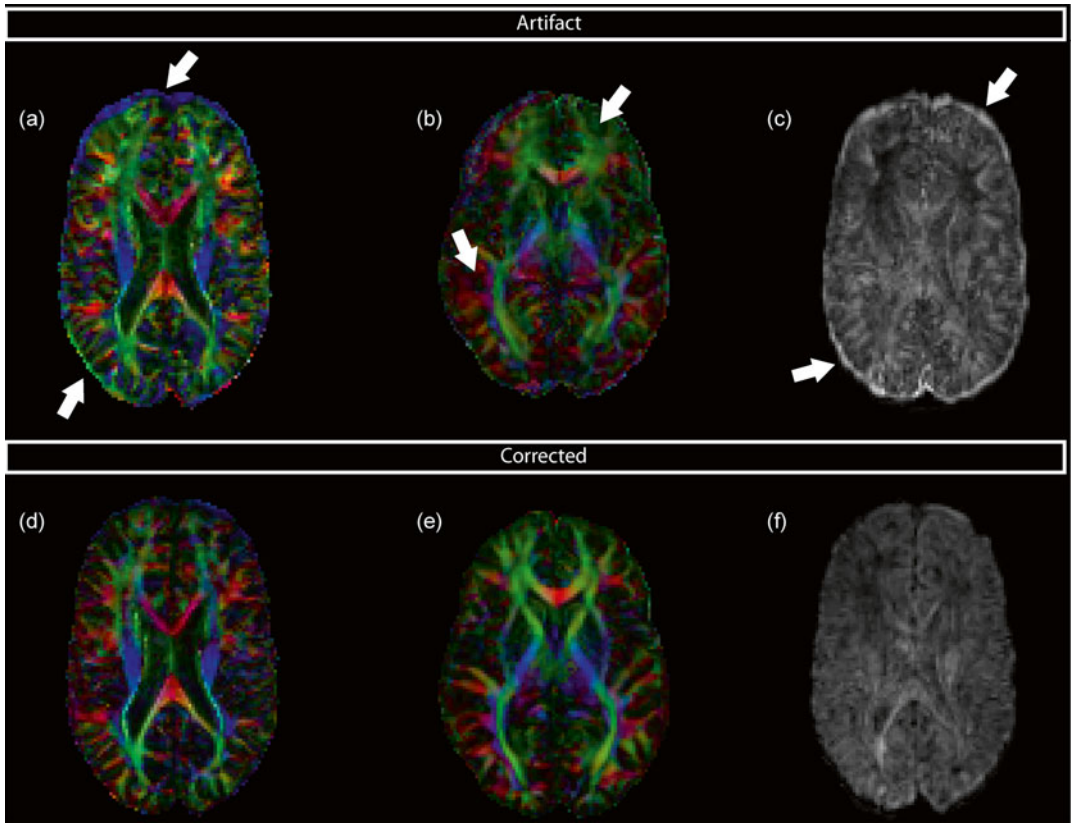

Fig. 7.5 Subject motion can be recognized on FA/DEC maps by a bright rim (**a**) or an overall change of FA (**b**). (**c**) When plotting the standard deviation across all DWIs, bright rims at brain edges indicate misalignment. (**d–f**) show the same maps, corrected for subject motion

with orientational bias at the periphery of the brain, but this will, in contrast to misregistration produced by eddy currents, appear on all sides of the brain (Fig. 7.5a). In other cases, overall changes in FA or MD can be observed (Fig. 7.5b). In addition to DEC maps, misregistration artifacts (resulting from either eddy currents or subject motion) can also be recognized by inspecting images of the standard deviation across the DWIs, in which the size and brightness of the rims at brain edges and tissue interfaces reflect the degree of misalignment (Fig. 7.5c). Recognition and correction of subject motion on these maps is not always straightforward and depends largely on the kind of motion (abrupt or gentle, small or large).

Image registration is commonly employed in diffusion MRI to correct for subject motion, and uses six parameters in total for translation and rotation. The corrected maps are visualized in Fig. 7.5d–f. The total transformation of eddy current distortion correction and subject motion are ideally applied at once on the original images [2]. A complication when dealing with registration of DWIs is that they contain directional information: diffusion gradients are applied in a specified direction. When the subject is rotated, one should rotate the *b*-matrix associated with each DWI. Neglecting to rotate the *b*-matrix can lead to incorrect diffusion metrics and erroneous tractography [13].

Interslice Instabilities

Origin

A specific type of motion artifact is interslice instability. This is discussed separately, since it only arises when motion occurs during an acquisition in which slices are scanned interleaved, i.e., even and odd-numbered slices of an EPI volume are collected sequentially (so first slices 1, 3, 5… and subsequently slices 2, 4, 6…).

Recognition and Correction in Acquisition Stage

Although it seems straightforward, checking the raw data in orthogonal views other than the slice direction is often omitted. Interslice instabilities such as intensity differences between slices resulting from interleaved acquisition can be recognized on these orthogonal views, see Fig. 7.6a. Artifacts arising from the interleaved acquisition are visible in the corpus callosum and at the brain edges, and result in signal dropouts. The best way to prevent these artifacts if they are motion related is to properly immobilize the subject or to use prospective motion correction as discussed above.

Recognition in Image Processing Stage

Interslice instabilities can become visible on FA DEC maps. The influence of motion in combination with interleaved acquisition is illustrated in Fig. 7.6b, where the artifact becomes apparent in different brain regions, such as the corpus callosum.

Table Vibrations

Origin

Table vibrations are the result of low-frequency mechanical resonances of the system due to application of the diffusion gradients [14, 15]. Spatial phase ramps in the phase image occur when neighboring voxels move over a different distance. These phase ramps correspond with shifts in k-space that result in signal loss. The amount of signal loss for a standard *b*-value of 1000 s/mm^2 can be 5–17 %, and increases with the *b*-value. Moreover, the twice-refocused spin-echo sequence suffers more from these vibrations due to the even more rapid switching of the gradients [15]. So, although the TRSE sequence ameliorates the eddy current-induced distortions, one must ensure that it does not come at the cost of increased table vibration.

Recognition and Correction in Acquisition Stage

Table vibrations can result in localized signal loss, which is not a result of diffusion. The movement resulting from vibration is primarily directed in left–right direction, and the artifact is therefore visible in DWIs with a large component of the diffusion gradient in the left–right direction.

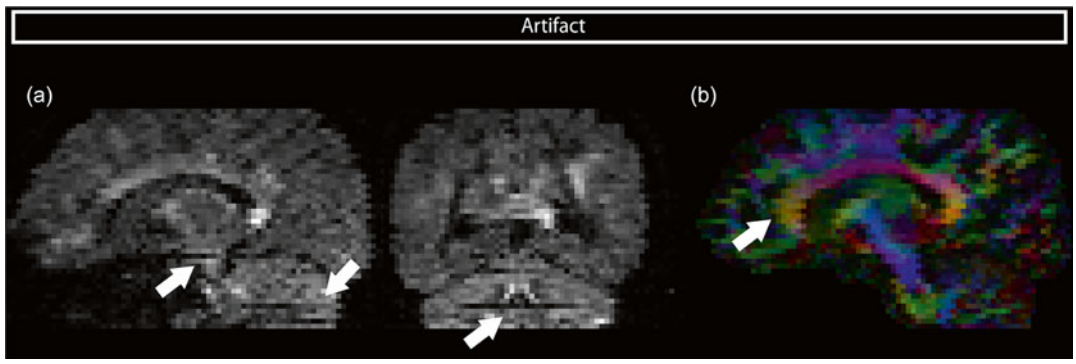

Fig. 7.6 (**a**) Interslice instabilities might not be visible on the axially interleaved acquisition plane, but becomes visible on the orthogonal planes in a DWI volume. (**b**) DEC map with interleave artifact

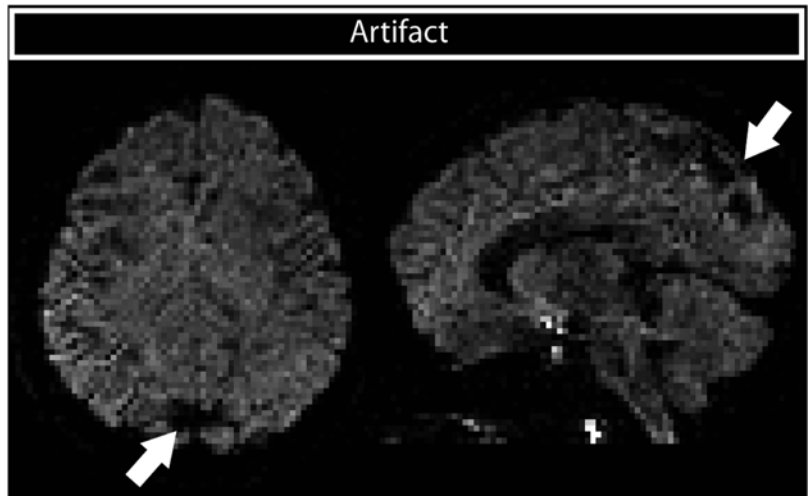

Fig. 7.7 Signal dropouts in DWIs with a large component of the diffusion gradient in *left–right* orientation resulting from table vibrations

Figure 7.7 illustrates this signal loss in a left–right sensitized image. When the region of signal loss overlaps with pathology, important diagnostic information can get lost.

Most diffusion protocols do not acquire the whole k-space, but use partial coverage instead to shorten TE which reduces scan time and increases SNR. In case of partial k-space acquisitions, vibrations could move the center of k-space out of the scanned k-space, resulting in severe loss of information for proper reconstruction of the DWI. Several acquisition options exist to reduce vibrations. Most conveniently, a mechanical decoupling of the patient table and gradient coils would reduce the vibrations themselves. This is, however, not a user acquisition choice as such, since this is determined by the vendor when designing the scanner. Second, full k-space coverage avoids this issue, generally at the expense of increases in TE [14]. At the expense of longer scan times, one could opt for a longer TR which would allow for the decay of vibrations between subsequent excitations.

Recognition and Correction in Image Processing Stage

Quantitative measurements such as FA and MD can be influenced by local signal dropouts in DWIs. In DEC maps, areas of the artifact can have artificially high FA in left–right orientation as can be seen in Fig. 7.8a. To improve the reliability of diffusion measures such as FA, a tensor fitting approach should be used that can account for the influence of this signal dropout. One possibility is to include the influence of the artifact as co-regressor in the tensor estimation [14]. The result of data correction can be appreciated in Fig. 7.8b. When one is not very familiar with these color-coded DEC maps or when pathology is involved, it might be hard to recognize areas of artificially high FA. In such cases, residual maps, which represent the difference between the actual measurement and the prediction after fitting the tensor model to the data, can illustrate the artifact more specifically. Signal dropouts in one or a few DWIs generally cause the tensor fit to be less accurate in those regions, which causes locally higher residuals (Fig. 7.8c). After correction, the residual map does not show the vibration artifacts anymore (Fig. 7.8d).

Pulsation

Origin

Even when the subject lies still, motion of brain tissue occurs due to the inflow of arterial blood following cardiac systole. These displacements are in the order of 1 mm and cannot be considered as simple rigid body motion as different brain regions have different displacement profiles. The largest motion can be observed in inferior

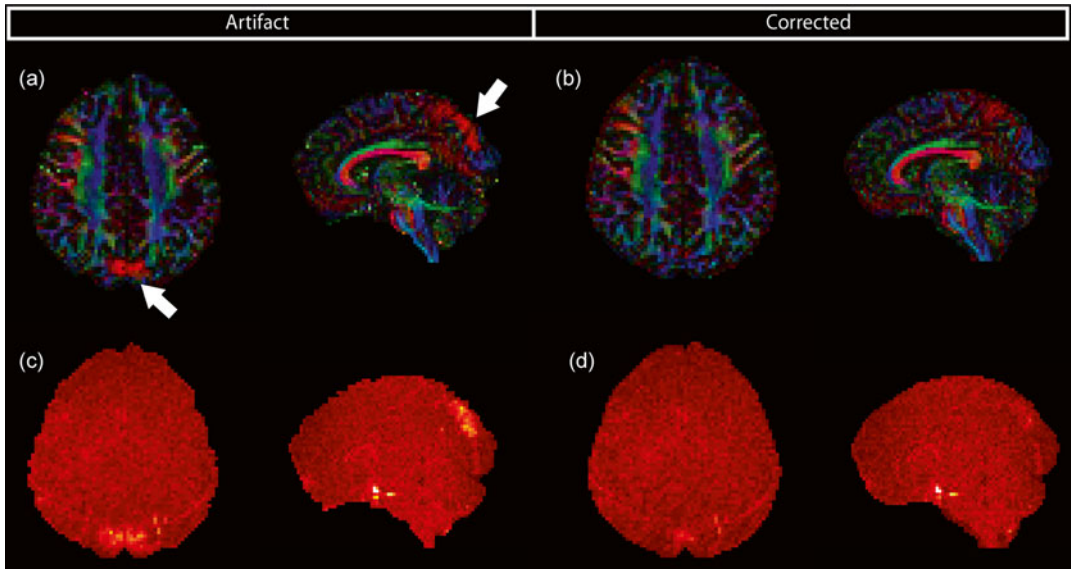

Fig. 7.8 (**a**) Areas of artificially high FA in *left–right* direction resulting from vibration artifacts. (**b**) Same FA map after correction for the vibration artifact by accounting for signal dropouts in tensor estimation. Mean residual map of the tensor fit (**c** and **d**) gives an indication of data quality and is sensitive to artifacts (**c**)

regions of the brain that move mostly along the inferior–superior direction [16]. Pulsation can be recognized for example around the lateral ventricles and brainstem. Two complications arise in further DTI analysis due to these pulsations. When DWIs are acquired in different stages of the cardiac cycle, they will have different local deformations, which results in local misregistration of structures between successive images. Furthermore, incoherent intra-voxel motion leads to additional signal attenuation [17–19].

Recognition and Correction in Acquisition Stage

The raw images can be used to detect local deformations, which are most pronounced in the region of the brain stem. Due to the differential contrast and eddy current-induced distortions between DWIs, it is hard to determine whether any observed deformations are caused by pulsation. When multiple non-DWIs are acquired, looping through the raw images at a high frame rate (e.g., 10 fps) may already illustrate the effect of cardiac pulsation.

As there is a direct mathematical relation between the image and the k-space, any artifact in the image is also present in k-space. Pulsation can result in dispersion or corruption in k-space leading to signal dropouts in the image. Holdsworth et al. [20] proposed the use of k-space entropy as a measure for k-space dispersion, where images with higher entropy than a given threshold value are defined as corrupted. Once a threshold is set, any corrupted slices can then be re-acquired later in the scan without the need for user input. Although this provides an automated method, the implementation requires online processing of the acquired data, and therefore nontrivial alterations to the scanner software.

To prevent the pulsation artifact from occurring in the acquired data, it is possible to acquire images only during several phases of the cardiac cycle, called cardiac gating. By ensuring that each slice is scanned during diastole, where there is little pulsatile motion, it is possible to acquire images that are unaffected by pulsation [21]. Although effective, gating comes at the cost of increased scan time, since there are periods in the cardiac cycle where no images can be acquired. In general, pulsation affects regions at and below the level over the corpus callosum [22]. With this knowledge, Nunes et al. [23] devised an

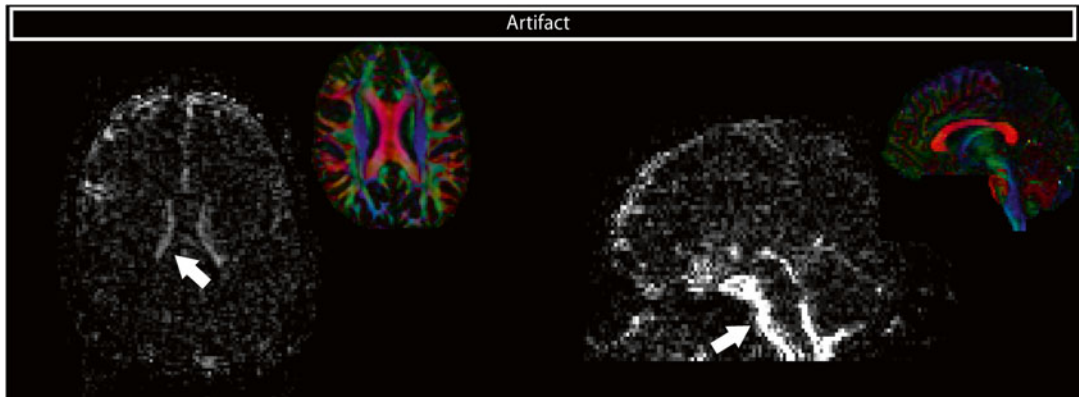

Fig. 7.9 Standard deviation across all non-DW (B_0) images shows high signal variability around the ventricles and the brainstem due to pulsation. FA DEC maps of the same slices are shown for anatomical reference

optimized acquisition setup where these inferior areas are scanned in the diastolic phase and supracallosal slices during the systolic phase. Using this setup they demonstrated a decrease in scan time of 30 % compared to the traditional cardiac-gated scan, while obtaining the same artifact-free images. Most MR vendors provide a cardiac gating option in their DWI sequences, making this a very convenient solution to pulsation artifacts, albeit at the expense of increased scan time.

Recognition and Correction in Image Processing Stage

Plotting the standard deviation across the non-DWIs for each voxel can show a high variability near moving regions, such as the medial parts of the brainstem and the lateral ventricles, due to pulsatile artifacts (Fig. 7.9).

On top of local misalignment artifacts, intravoxel dephasing leads to additional signal attenuation, which will be interpreted as increased diffusion. This will bias the diffusion tensor estimate and will influence anisotropy measures and tractography results [17].

Tensor estimation in the presence of cardiac-induced artifacts can be improved by more advanced tensor estimation methods that recognize corrupted data as outliers. Robust estimation approaches such as Robust Estimation of Tensors by Outlier Rejection (RESTORE, see also Chap. 6 and [24]) and Robust Extraction of Kurtosis INDices with Linear Estimation (REKINDLE) [25] can be very effective in obtaining diffusion tensor parameters that are not affected by cardiac-induced artifacts.

Susceptibility-Induced Distortions

Origin

Magnetic susceptibility refers to the degree of magnetization of an object in response to an applied magnetic field. Tissue is diamagnetic, which means that it creates a magnetic field in opposition to the externally applied magnetic field. The magnetic field in the tissue will therefore be slightly lower than the scanner magnetic field. Different tissues have different magnetic susceptibilities, which makes the magnetic field (B_0) dependent on the shape and composition of the body part that is imaged. Susceptibility differences are particularly large in regions where air-filled sinuses are close to bone or tissue, such as in the temporal and frontal lobe. EPI images are prone to these susceptibility differences in particular, since a whole volume is acquired within a single excitation. In clinical practice, k-space is filled as displayed in Fig. 7.10a. The locally altered magnetic field will cause a local displacement of the object in the PE direction [26, 27]. More specifically, the geometric distortions scale linearly with the FOV in the PE direction, and with the time between two consecutive points in the PE direction.

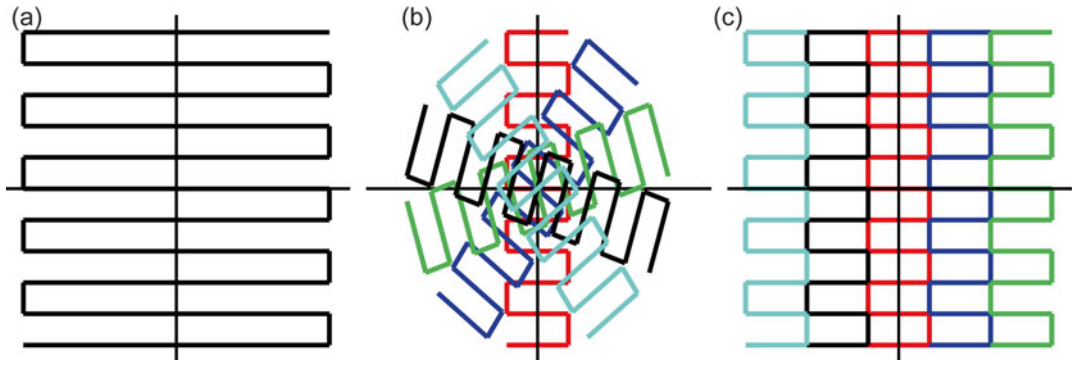

Fig. 7.10 (**a**) k-space trajectory of single-shot EPI, where the entire k-space is read after a single excitation. (**b**) Short-axis propeller EPI, where rotating "blades" in k-space are read out after each excitation. (**c**) Readout-segmented EPI reads out "blinds" of k-space in each excitation

Recognition and Correction in Acquisition Stage

The distortions may cause regions of signal "pile up," where the signal of several voxels is compressed into one voxel (Fig. 7.11b), or signal "smearing," where the signal from one voxel is stretched over several voxels (Fig. 7.11a).

To compensate for B_0 inhomogeneities, an additional magnetic field can be created by running currents through small coils [28]. This is called shimming, and the coils used are called shim coils. In MRI brain imaging, there is always some form of shimming. Mostly, linear shimming is used, also called first-order shimming, where additional magnetic fields along x, y, and z are applied to make the B_0 field more homogeneous. Higher-order shimming is also possible, where second- or third-order fields are applied to account for highly nonlocalized magnetic inhomogeneities [29]. These higher-order shimming methods require additional coils and software, but are widely available in dedicated brain imaging centers.

In the presence of an object that causes an inhomogeneous B_0 field, shimming is the accepted method to correct these inhomogeneities. However, the acquisition of the DWIs can be adjusted such that the effects of inhomogeneities are minimized. One way to do this is by parallel imaging methods, e.g., SMASH, SENSE, or GRAPPA, which were designed to speed-up MR image acquisition by acquiring only parts of k-space, and then reconstructing the whole image [30–32]. The use of multiple receiver coils that detect the MR signal then provides the additional spatial information to reconstruct the complete image from an incompletely sampled, or undersampled, k-space. It is most efficient to undersample in the PE direction because this provides the largest speed-up. An additional benefit is that in EPI, this also reduces the image distortions caused by local field inhomogeneities, with higher parallel imaging factors giving lower distortions.

Another way to reduce image distortions is to change the way k-space data is acquired. Several pulse sequences have been designed that do this, including short-axis PROPELLER EPI (SAP-EPI, [27]) and readout segmented EPI (RS-EPI, [20]). SAP-EPI acquires multiple rotating and overlapping "blades" in k-space that together create a full k-space (Fig 7.10b). Instead, RS-EPI acquires several parallel adjacent "blinds" in k-space that combine to a full k-space (Fig 7.10c). However, these techniques require multiple blades or blinds to be scanned to construct a full k-space. Since the individual blades or blinds are acquired after separate excitations, this results in longer scan times. Recently, diffusion-weighted vertical gradient and spin-echo EPI was proposed, which basically acquires all the RS-EPI blinds after a single excitation, significantly increasing the imaging speed compared to RS-EPI [33]. Although these techniques provide

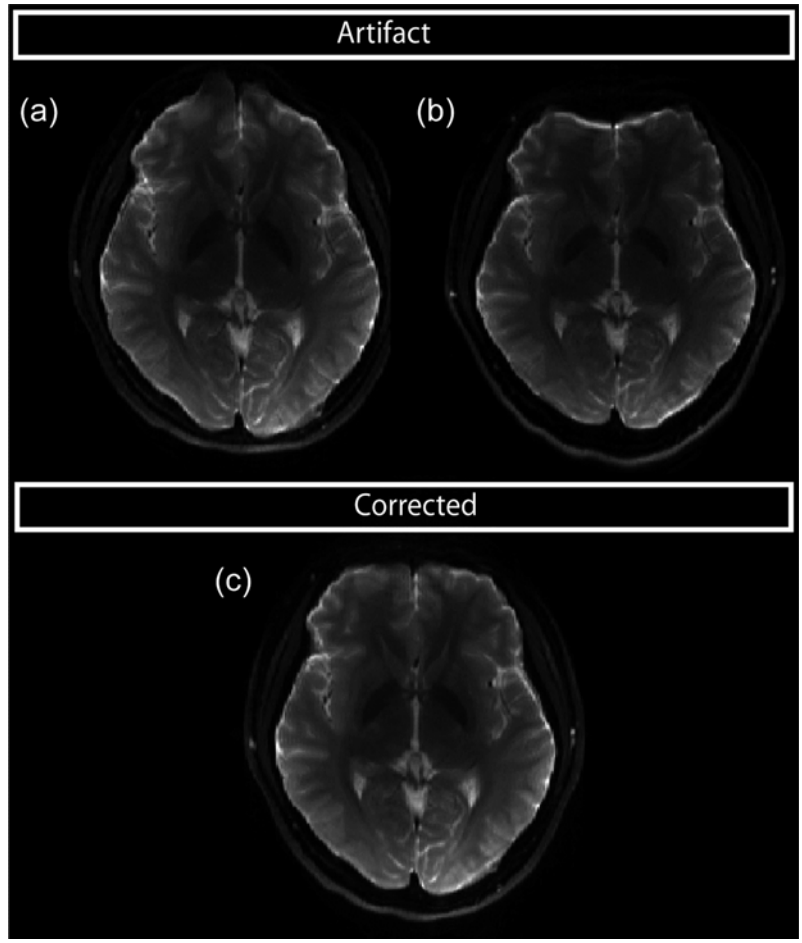

Fig. 7.11 (**a**) Susceptibility-induced distortions when using negative EPI blips, displacements toward the front. (**b**) Positive EPI blips result in displacements posteriorly. (**c**) Corrected data. [Courtesy of Dr. Roland Bammer, Stanford University]

a higher image quality and have been shown to provide improved diagnostic confidence [34], they are not widely available and thus not widely used in diffusion MRI.

Recognition and Correction in Image Processing Stage

Deformations of the DWIs can be recognized when fusing them with an anatomical image which is less geometrically distorted. Figure 7.12a shows the overlay of the DEC map with a T1 image after rigid registration, showing a clear mismatch between the two images.

There are several "unwarping" methods that can be used to deal with these distortions in image processing stage. Most of these methods, however, require additional image acquisitions and as such are not purely post-processing strategies. One option is distortion correction with the use of a field map. An example field map is shown in Fig. 7.13, which illustrates the deviation of B_0 from the Larmor frequency. Spatial variations in B_0 cause the distortions, and knowing these variations enables us to calculate the shift per voxel and compensate for the shift [35]. A drawback of this method is that it cannot correct for signal "pile up," because the intensity of that particular location is then a mix of intensities from different voxels, and this is impossible to resolve [36].

An alternative method is to acquire two datasets with opposite PE direction (and thus oppositely directed distortions), so that one could reconstruct the undistorted image from these two data sets [37]. This is called the reverse polarity gradient method because of the opposite polarity

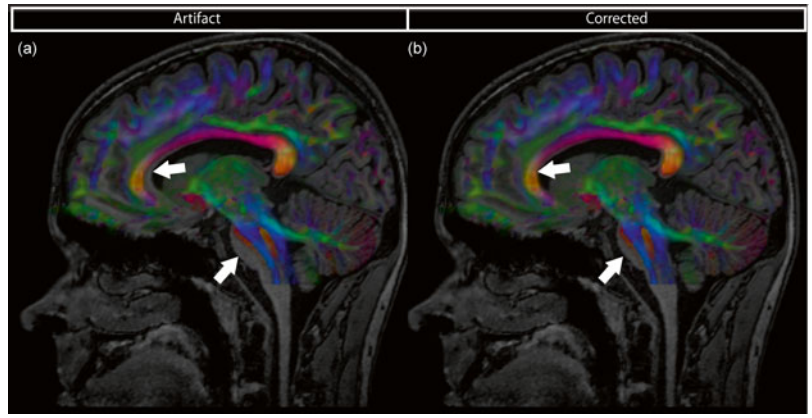

Fig. 7.12 Color FA map derived from DW-MRI data overlaid on anatomical undistorted image. Due to EPI deformations in the DWI, there is a misregistration that is most obvious near the brain stem and corpus callosum (**a**). (**b**) Result after correction by non-rigid image registration

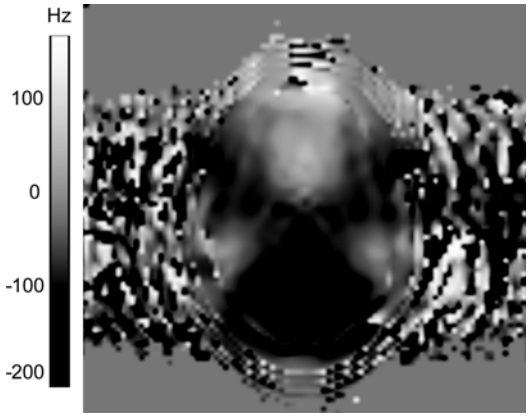

Fig. 7.13 Field map with the gray values representing B_0 variations in Hz

of the PE gradient in this method. The benefit here is that regions with signal "pile up" in one image have signal "smearing" in the other image, and vice versa. Recall Fig. 7.11a, b. This overcomes the main drawback of the field map method. A downside to this method is that more images should be acquired, increasing the scan time.

Finally, an undistorted image (e.g., T1, T2) can be used to unwarp residual EPI distortions present in DWI data by non-rigid image registration [38], see Fig. 7.12b.

Conceptually, the last two correction methods could be combined, where the registration to an undistorted image fine-tunes the images corrected with the field map of reverse polarity method.

Nyquist Ghosting

Origin

The origin of Nyquist ghosting is hardware related. In the scanner, there is a time delay of microseconds between the application of the readout gradient and the actual acquisition. This leads to a shift of the data in k-space, which corresponds to a phase ramp in image space: the "ghost" [39]. The ghost arises due to a mismatch between readout from positive and negative readout directions.

Recognition and Correction in Acquisition Stage

Ghosting can immediately be recognized in the raw images as a copy of the object, shifted by half of the FOV (see Fig. 7.14).

Multiple correction methods have been proposed and generally fall into methods that require additional acquisitions (e.g., a reference scan) or those that do not. To correct for the shift in k-space, the reference scan is composed of multiple readouts through the center of k-space which can be used to determine the difference between positive and negative readouts. This difference—acquired without diffusion weighting—can then be used to correct all acquired non-DWI and DWIs in the rest of the session [40]. Although this is a very quick method, the downside is that it is not suitable for longer DWI scans, which are more and more

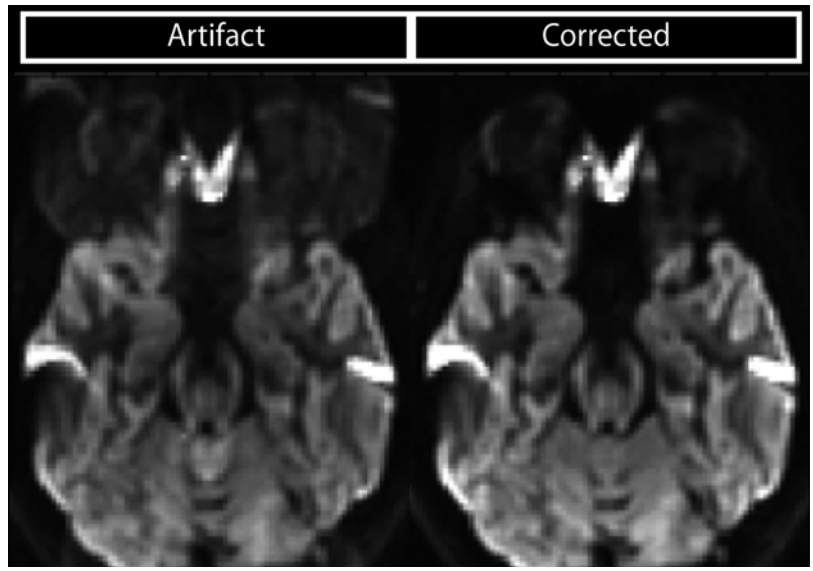

Fig. 7.14 Nyquist ghosting can be recognized as a copy of the image that is shifted over half the FOV

common to accommodate HARDI (see also Chap. 13). Subtle changes in the MR system during the scan may render the reference acquired at the beginning inadequate for ghost correction at the end of the scan. To resolve this, reference scans can be acquired intermittently during scanning to update the correction parameters. If multiple non-DWIs are acquired and these are spread out over the session, these references can be scanned during the "dead time" because of the missing diffusion-weighting gradients. Mostly, the scanner has one fixed method to do ghost correction, which leaves the user with no alternatives. However, if these "standard" methods prove insufficient to fully correct for ghosting, one should realize there are alternative methods that could prove to be beneficial.

Recognition and Correction in Image Processing Stage

Alternatively, one can use the acquired images themselves to do ghost correction. By generating separate images from the odd and even echoes, phase maps of those two images can be generated. Under the assumption that phase changes have a low spatial frequency, the two phase maps can be used to calculate a phase correction and reconstruct one final un-ghosted image [39, 41].

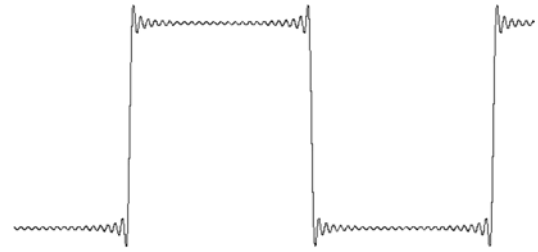

Fig. 7.15 Ringing artifact around large steps in intensity

Gibbs Ringing

Origin

Gibbs ringing is a common artifact in MRI but is often overlooked in diffusion MRI applications [3]. To describe steep intensity transitions in an image (e.g., cerebrospinal fluid, CSF, next to white matter), one needs high frequencies. When acquiring k-space, however, the acquisition window is not infinitely large but rectangular. High frequencies beyond the acquisition window are assumed to be zero. This leads to the well-known ringing artifact in the image [42], see Fig. 7.15.

Recognition and Correction in Acquisition Stage

Gibbs ringing artifacts are the most prominent in the non-DW image because the intensity differences are

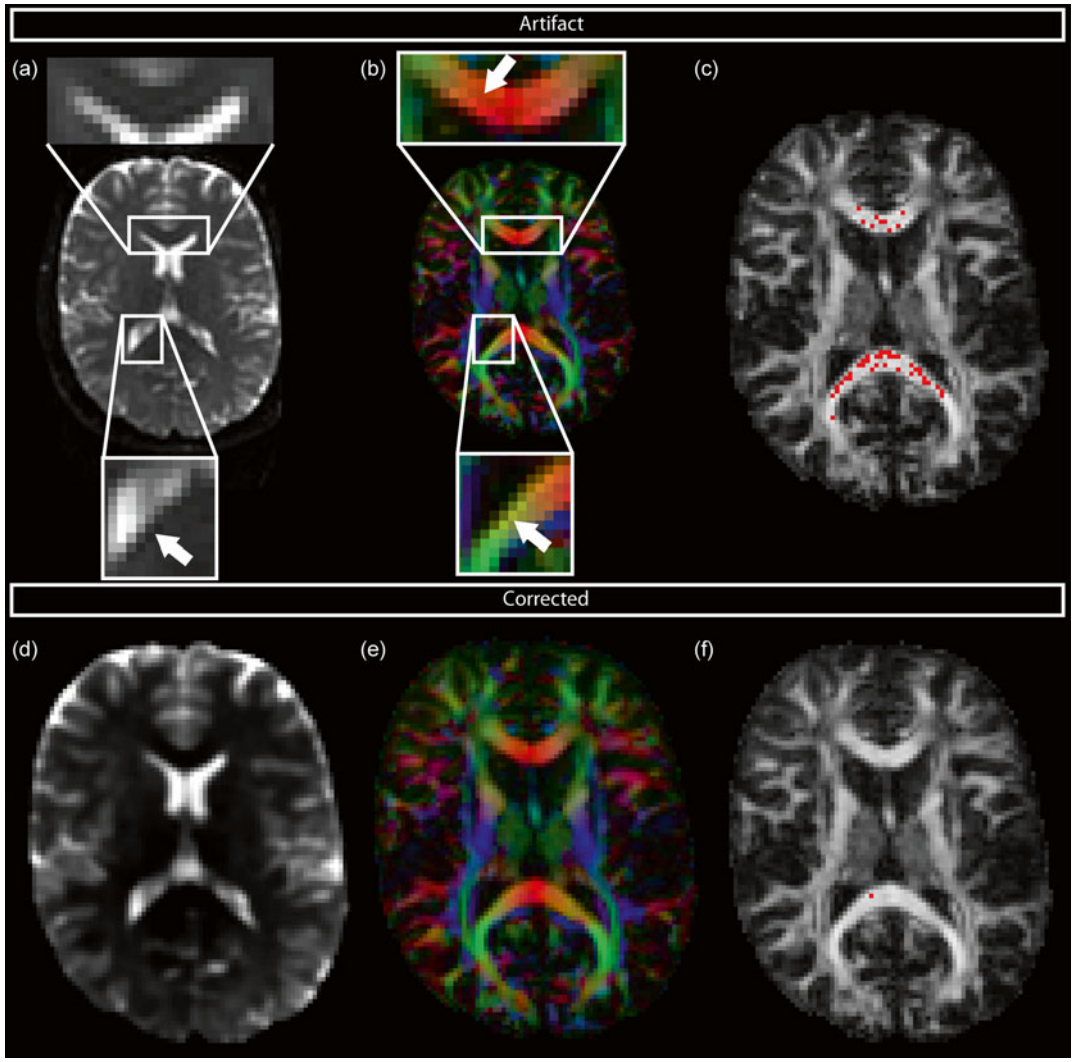

Fig. 7.16 Gibbs ringing artifact. (**a**) B_0 image shows the artifact at the location of high intensity gradients. (**b**) DEC map with Gibbs ringing artifact. (**c**) PIS map, indicating regions where the $b=0$ image has smaller intensity than the DWIs. (**d**–**f**) show the corrected images

largest in this image, as shown in Fig. 7.16a at the interface of CSF and brain tissue.

Sampling a larger interval in k-space (with proportionally more points in k-space) for a fixed field-of-view will reduce the pixel width, and therefore the spatial distance over which the ringing propagates. Running two scans with different k-space intervals can give insight in the Gibbs ringing artifact, but this is not often an option due to prolonged acquisition time.

Recognition and Correction in Image Processing Stage

The Gibbs ringing artifact can also be recognized on DEC maps as intensity variations, see Fig. 7.16b. Since diffusion will lead to signal decay, the non-DW image should always have a larger intensity than DWIs for each voxel. Due to Gibbs ringing artifacts, amongst others, this is not always the case. Visualizing the occurrence of these physically implausible signals (PIS)

overlaid on an FA map indicates at which locations these artificial signals occur, as shown in Fig. 7.16c [3].

Gibbs ringing artifacts have influence on diffusion estimates, and it is therefore desirable to correct for these artifacts. There are several approaches that deal with Gibbs ringing artifacts, e.g. [43–47]. The total variation (TV) approach, for example, calculates a corrected image by including a term that preserves edge information in the image and meanwhile minimizes the contribution of large adjacent intensity differences [46].

Chemical Shift Artifact

Origin

When placed in a magnetic field, protons in fat have a different resonance frequency than those in water. During acquisition of the MR images, the frequency and phase of the signal are used for spatial encoding of the signal. The difference in frequency of fat and water can therefore be interpreted as a difference in position. In EPI images, fat containing structures are therefore shifted from their true positions in the phase-encoding direction.

Recognition and Correction in Acquisition Stage

On a 3T clinical system, the fat/water chemical shift can approach 5 cm [48]. When imaging the brain, the largest fat component can be found between the skull bone and skin. The hyperintense band of the fat signal can be visible on raw DWIs, as shown in Fig. 7.17a.

To ensure there is no fat signal to disrupt the image, several "fat suppression" methods have been proposed that can be generally classified into three different methods: specifically exciting the water protons; saturation of the fat magnetization; moving the fat signal away from the imaged object. The first method was initially proposed by [49] as a spectral-spatial (SPSP) selective excitation, where interplay between switching slice-selection gradients and RF pulse excites only the water protons. This is the most effective method in terms of fat suppression, but suffers from two main drawbacks: (1) Due to hardware constraints on clinical systems (mostly the gradient slew rate), slice thicknesses is limited to around 2.4 mm or thicker; (2) The SPSP pulse can be relatively long in order to get a good fat suppression, thus increasing scan time. The second method uses an RF pre-pulse, to null the fat magnetization before the actual water excitation.

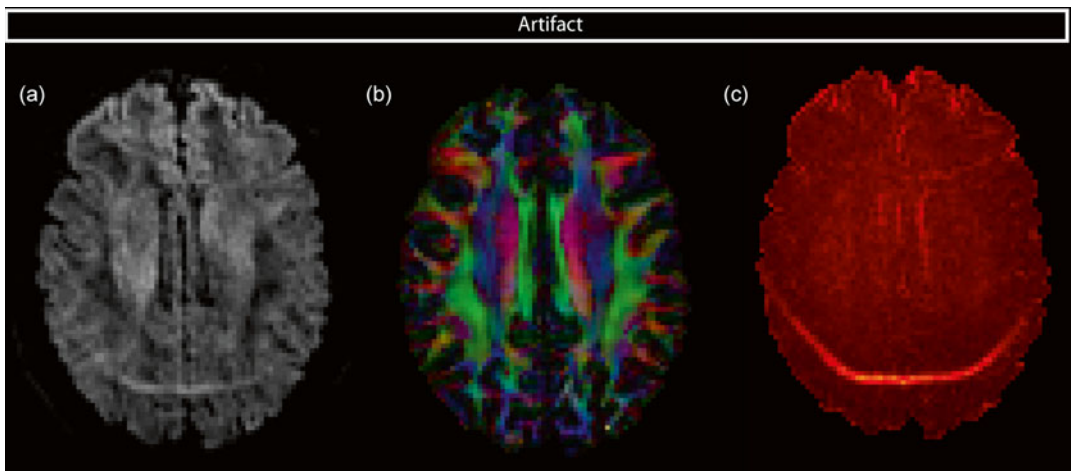

Fig. 7.17 Fat band is sometimes visible as bright intensity band on raw images (**a**), whereas it is often missed on DEC maps (**b**). Residual map clearly shows the chemical shift artifact (**c**)

Two pre-pulses exist: (1) An inversion pulse (e.g., SPIR, [50]), where the fat magnetization is inverted and the actual excitation is done at the time that fat has zero magnetization. The time between inversion and excitation is called the inversion time, and tuning this is critical for good suppression. (2) The fat is excited and then "spoiled" before excitation (CHESS, [51]), resulting in no magnetization of fat. Unfortunately, at current clinical field strengths of 1.5T or 3T, this approach commonly provides incomplete fat suppression (as illustrated in Fig. 7.17a and a slight increase in scan time). The third method uses slice-selection gradient reversal (SSGR) [52, 53]. Due to relative differences in frequency, the slice of fat that is excited is shifted along the slice direction compared to the excited water. When opposite gradient polarities are used during the excitation and refocusing RF pulse, the fat slice will in turn be shifted in opposite directions in the excitation and refocusing part. As a result, the volume of fat tissue that experiences both the excitation and refocusing pulse is very small, which means there is little signal from fat. This is shown schematically in Fig 7.18.

In a recent overview, Sarlls et al. [54] compared different fat suppression methods for twice-refocused DW imaging: CHESS, SSGR, SPSP, and a combined CHESS-SSGR approach. The SPSP and CHESS-SSGR methods performed similarly in terms of effective fat suppression and SNR, but the CHESS-SSGR combination resulted in a slightly shorter scan time.

Depending on the vendor, one or several of these fat suppression options are available. Even within one option, there are specific parameters that can be tuned to try and optimize fat suppression. In SPIR, for instance, the inversion time can be set for each scan. Alternatively, the difference between the water and fat resonance frequency can be set in SPIR, CHESS, and SPSP. Optimal values of these parameters are dependent on several scanner-specific settings, including the main field strength, gradient strength, and gradient slew rate, but are certainly worth investigating to provide proper suppression.

Recognition in Image Processing Stage

Insufficient fat suppression can become visible on DEC maps, but this is not always obvious (Fig. 7.17b). The easiest method to detect these artifacts is by making a residual map of the diffusion tensor residuals, where the chemical shift artifact can be recognized as a bright band of higher residuals (Fig. 7.17c). It is difficult to correct for this artifact at this stage, and one should be careful with interpretation of the data in these corrupted regions. The locally biased tensor estimation can become apparent globally in tractography analyses.

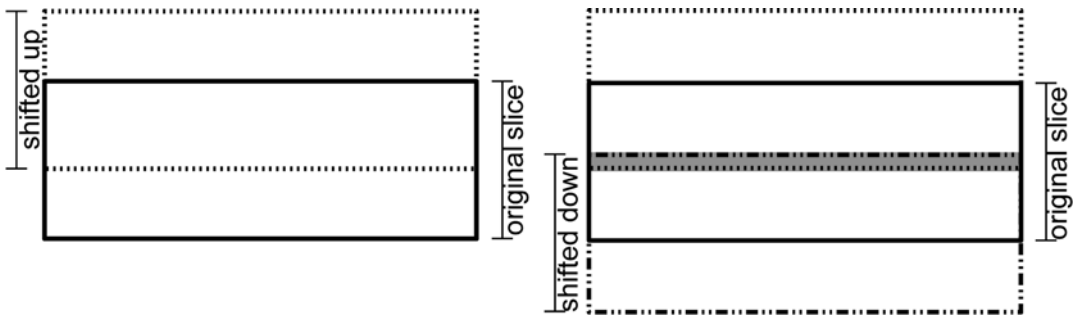

Fig. 7.18 Schematic representation of the slice-selection gradient reversal (SSGR) method. The *solid black line* indicates the spatial location of the slice of water that is excited. The fat slice that is excited is displaced with respect to the water slice along the slice direction (*shifted up*, *dashed line*). The refocusing pulse is then combined with a gradient that has an opposite polarity to that used in the excitation pulse. The fat volume that experiences this pulse is shifted downwards (*dashed-dotted line*). The overlapping area in the middle of the slice (*gray*) is the only part of the fat signal from this slice that will give an echo

Signal and Slice Dropouts

Origin

Signal dropouts can have many origins, such as gross subject motion, cardiac pulsation, strong local susceptibility difference (e.g., dental braces), and hardware problems, among others. Since the first three causes have been described at length previously, we focus here on the hardware-related problems. One example is a loose connection in the scanner, which can cause part of k-space to not be stored. Depending on the part of k-space missing, and the extent, this artifact can have various representations in the image. Alternatively, receiver calibration can be incorrect. Prior to scanning, the scanner performs a quick test scan to see what the maximum signal will be to calibrate the system. If this is set too low, points in k-space may have their intensities "clipped," resulting in artificial contrast differences in the image.

Recognition and Correction in Acquisition Stage

Given that hardware-related problems can present themselves as a broad range of image artifacts, the artifacts can be difficult to detect and their origins hard to pinpoint. On raw data, detection can best be done by looking for structural hypointense areas, such as slice dropouts, shown in Fig. 7.19. One should be aware, however, that not all dropouts are as obvious as this example, and the best way of detection is in the post-processing stage.

Recognition and Correction in Image Processing Stage

Signal dropouts are sometimes subtle and not always obvious to recognize on raw images or FA maps (Fig. 7.7). Residual maps of the tensor estimation are sensitive to dropouts, see Fig. 7.20. When fitting a tensor, the RESTORE

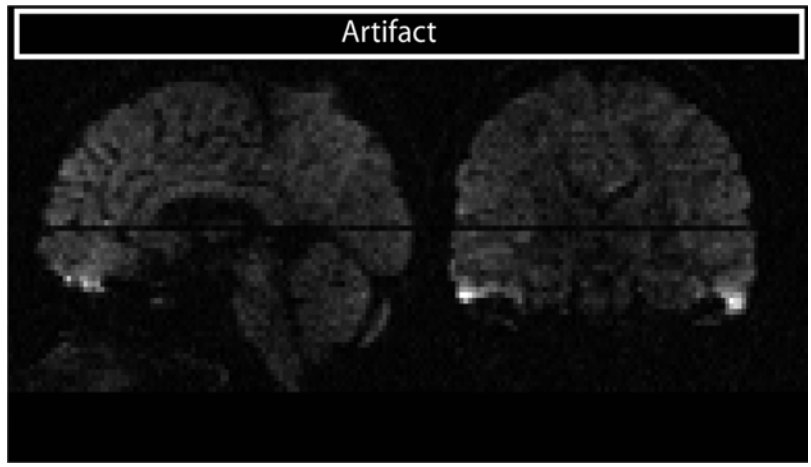

Fig. 7.19 Total slice dropout in the sagittal (*left*) and coronal (*right*) view

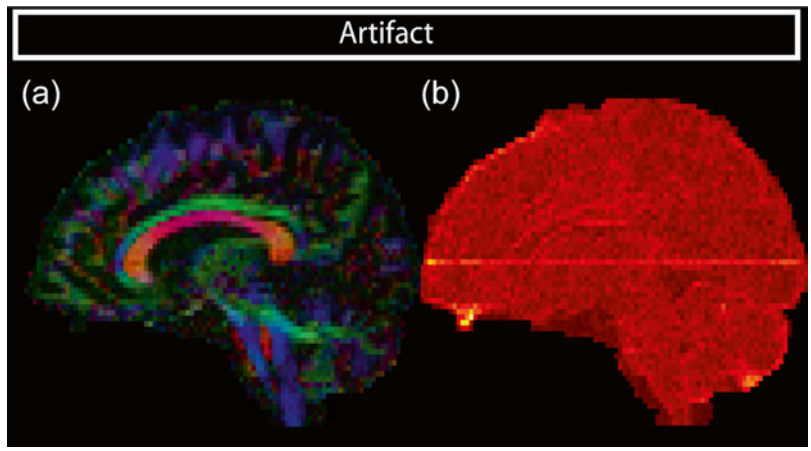

Fig. 7.20 (**a**) Slice dropouts are hard to spot on FA maps, but do influence diffusion measures locally. (**b**) On the tensor residual map, the slice dropout can well be recognized

and REKINDLE approaches can deal with these outliers by ignoring them during tensor estimation [24].

Quality Assurance

Several of the artifacts discussed in this chapter can be corrected for, either at the acquisition or the processing stage. As such, they do not limit the analyses of DTI data, but rather force the user to consciously consider the acquisition and processing steps prior to the analyses. Since the introduction of DWI and DTI, much research has been devoted to solve or reduce image artifacts. Eddy current-induced and susceptibility-induced image distortions, for instance, can now be addressed both by tuning the acquisition and the image processing side, with clear pros and cons to both options. In terms of the image processing steps described here, most software packages available to date provide users with adequate options to do these correction steps. Although there are various ways to correct for artifacts, it is of major importance to check quality requirements before acquiring data on clinical or research subjects, by using quality assurance (QA) tests.

QA and Phantoms

QA is concerned with the implementation of activities to fulfill quality requirements, such as comparison to a gold standard. Standard QA tests consist of gradient calibration (including linearity, uniformity, and agreement in amplitude), field mapping to minimize B_0 inhomogeneities, and eddy current compensation [55]. This is most commonly done by imaging phantoms with different gradient directions and *b*-values. Phantoms are suitable for validation of acquisition parameters, as well as diffusion measures and fiber tractography results [56–59]. It is important to quantify precision, accuracy, and reproducibility in diffusion MRI analysis. Vegetables (like asparagus [60]) or animal nerve structures (like rat spinal cord, garfish, or lobster nerves [61, 62]) are sometimes used. However, in such organic matter it is more difficult to manipulate the natural geometry of the tissue in order to reflect more complex microstructural configurations (i.e., to construct interdigitated crossing fibers), and the diffusion properties of such organic material may change over time. Hardware phantoms can be made of isotropic media (e.g., liquids of known diffusivity) or anisotropic media (e.g., capillaries or artificial fibers). The properties of these phantoms are tuned to resemble human white matter. Liquids of known diffusivity (e.g., Dodecane) can be used to calibrate absolute gradient power. Glass capillaries or PTFE (Teflon) capillaries [63] are rigid, while for example hydrophobic fiber materials (with high FA, [64]) can be adapted to the desired geometry to create artificial fiber phantoms.

Quality Control

One important aspect of quality assurance and control is that the user should always remain critical when employing automated correction methods. One example could be the use of robust estimation procedures on data with artifacts. When a DW image is partly corrupted, RESTORE or REKINDLE might classify those corrupted voxels as outliers, and disregard them in tensor estimation. However, if a large portion of the image is corrupted, the image might not be correctly registered, which could mean that the "good" voxels that are included in tensor estimation are also unreliable because they provide diffusion information about different spatial locations. An example of this is shown in Fig. 7.21 for a DW image (Fig. 7.21a) simulated to have an interleaved artifact (Fig. 7.21b). The coregistration of such an image to the other images will not be accurate. Residual maps (Fig. 7.21c) will not show this. However, the number of outliers detected is a very good indicator of a subtle image artifact (Fig. 7.21d). As shown here, the interleaved artifact only causes 7 % of all brain voxels to be judged by RESTORE as outliers, even though at least half of all WM voxels are misaligned and therefore provide erroneous information. This is because misregistration of voxels within the WM might not provide a strong

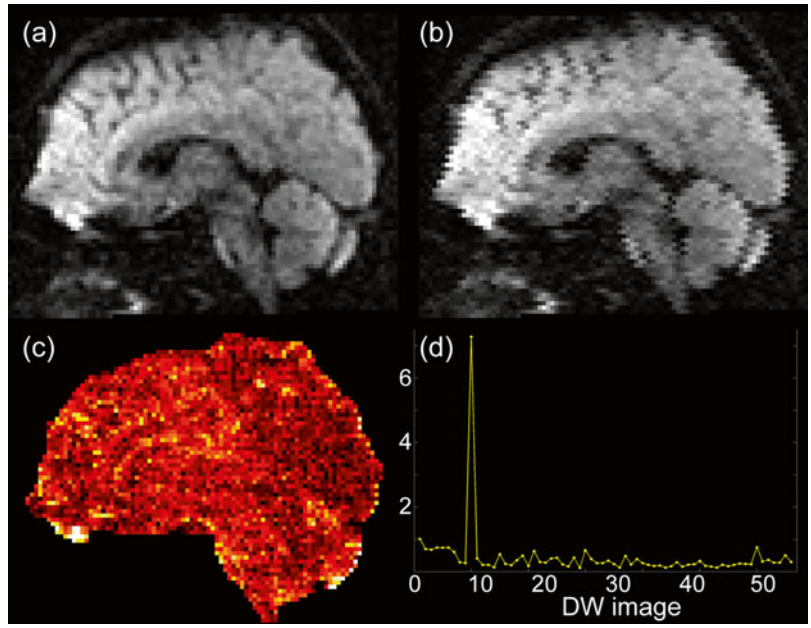

Fig. 7.21 Importance of manual data quality assurance. One DW image (the tenth) shown uncorrupted (**a**) and with interleaved artifact (**b**). The tensor residual map at this slice (**c**) does not show the presence of any artifact. However, outlier percentages per DW image (**d**) strongly indicate an artifact. Interesting, only 7 % of all brain voxels are classified as outliers, whereas roughly half of the image is misaligned

enough contrast difference to be classified as artifact. In such cases, one could argue to remove the entire DW volume from further analyses to ensure they are not negatively affected.

Implications for Further Analysis

Effects of Bad Quality Data on Quantification

MD and FA are, amongst others, important quantitative measures that can be used in subsequent ROI analyses, voxel based analyses (VBA), and tractography analyses (See Chaps. 6, 7). Comparison of these values between different groups can reveal associations with clinical parameters, which has been the focus of a large amount of studies. Artifacts can influence the diffusion measures, as shown in Fig. 7.22, where FA values (top two rows) and MD values (bottom row) are locally altered. Furthermore, artifacts can complicate proper analyses in particular areas. It is well known that structures in the orbitofrontal cortex, for example, are prone to susceptibility artifacts, which makes these white matter areas less accessible to study. This might attribute to the fact that larger white matter tracts with densely packed neuronal fibers tend to be studied more than less prominent pathways. For example, the corpus callosum is a pathway that can readily be identified, which makes this pathway better suited for investigation in quantitative studies [65]. We have seen that most artifacts cause difficulties in the registration of individual DWIs, which will eventually affect any subsequent analysis. One should be aware that the corpus callosum, for example, can also be corrupted by artifacts, such as susceptibility distortions (Fig. 7.10), Gibbs ringing (Fig. 7.13), and interleave artifacts (Fig. 7.15).

Effects of Bad Quality Data on Tractography Results

With tractography, the architectural configuration of white matter fiber bundles can be investigated in vivo (See Chap. 11). For DTI tractography, the local first eigenvector is typically used for tract propagation (Chap. 6). Besides noise and partial volume effects, data artifacts and lack of proper

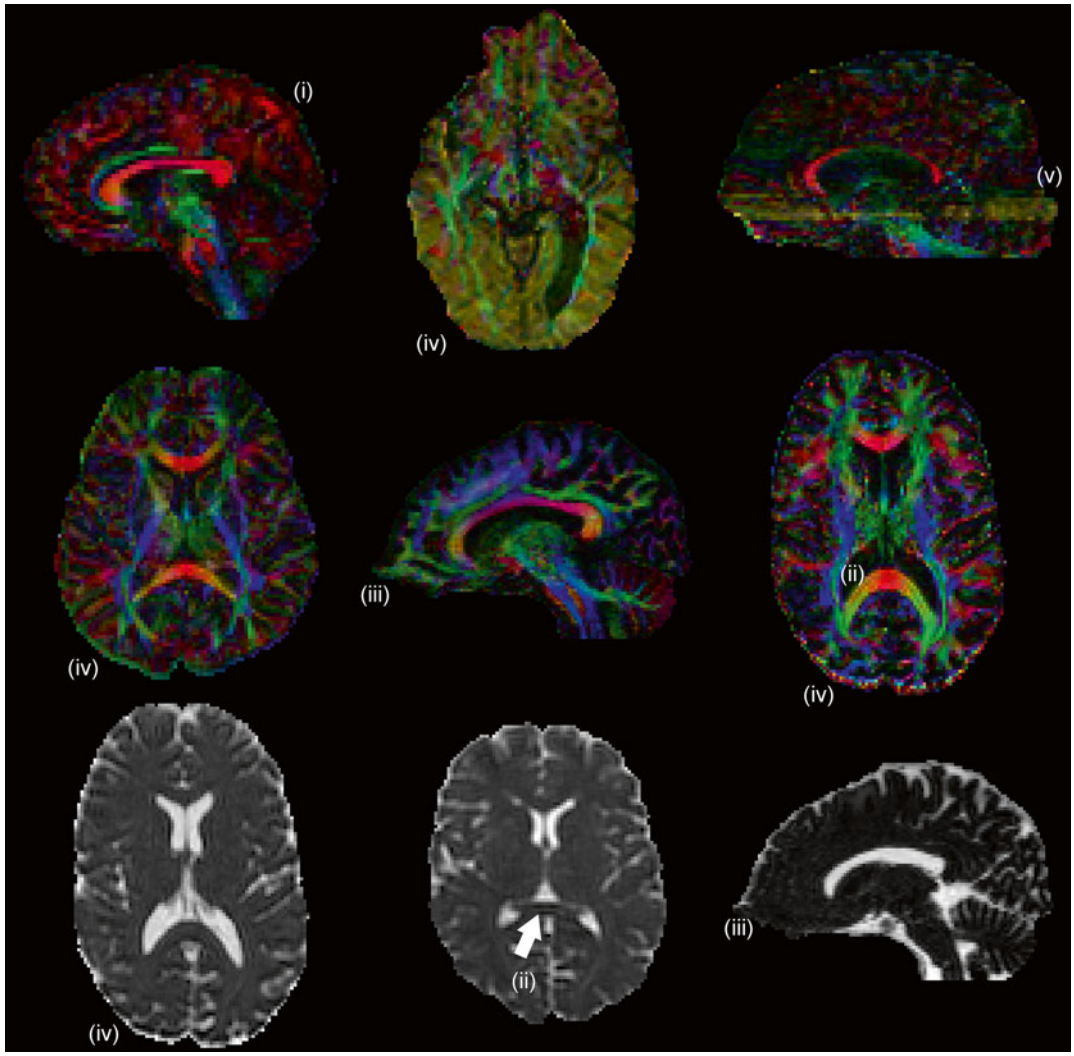

Fig. 7.22 Effects of bad quality data on quantitative measures (FA *top two rows*, MD *bottom row*), showing (**i**) vibration artifact, (**ii**) Gibbs ringing, (**iii**) Susceptibility distortions anterior, (**iv**) Motion and eddy current distortions, (**v**) interleave artifacts

correction can severely confound local fiber configurations and therefore fiber tractography results. Figure 7.23 shows examples of the influence of bad quality data on tractography results using a deterministic algorithm, for different artifacts. The results clearly show the deviation in the reconstructed pathways when proper correction methods are not taken into account. Pathways can have a different geometry and may even terminate in other brain areas [66]. To date, tractography is mostly used for analyses in which quantitative measures along tracts are compared between patients and controls, to study which areas in the brain are connected, and for neurosurgical planning. It is of major importance to assure data quality before acquisition and correct for artifacts during acquisition and image processing to ensure the reliability of all subsequent analyses.

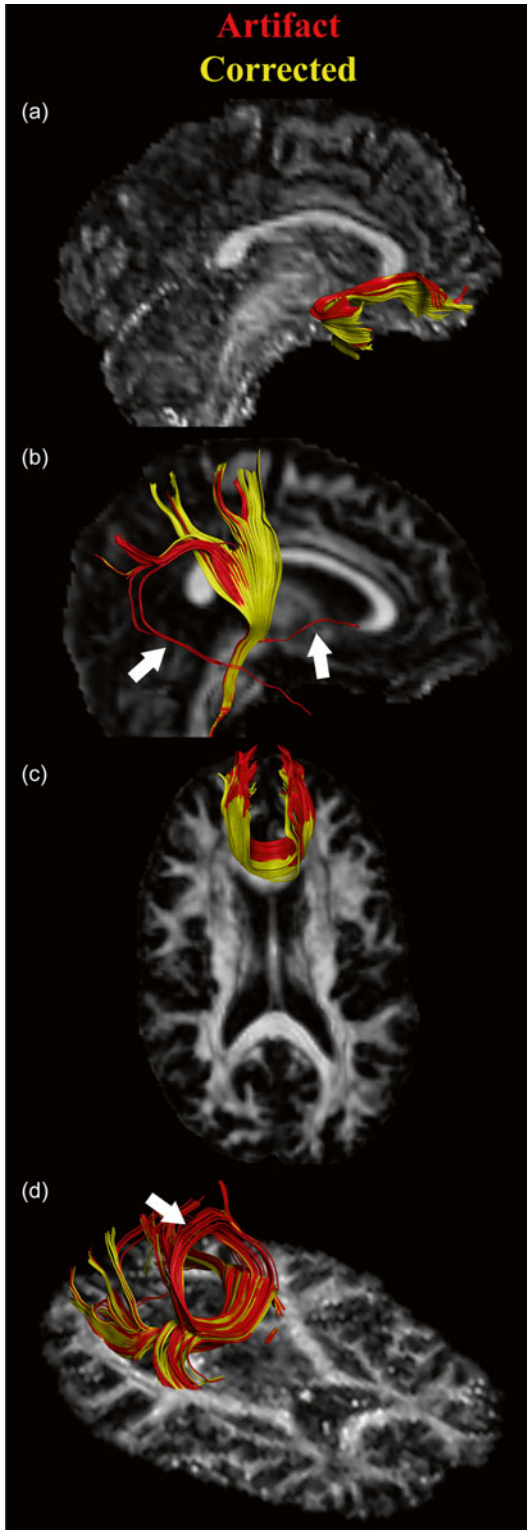

Fig. 7.23 Effects of bad quality data on tractography results. (**a**) Tractography of the uncinate fasciculus before (*red*) and after (*yellow*) motion and eddy current distortion. (**b**) Corticospinal tract in a set where we simulated an interleave artifact (*red*) and in the "ground truth" set (*yellow*). The artifact results in clearly artificial tracts. (**c**) Frontal projections of the corpus callosum in a dataset with susceptibility distortions (*red*) and the corrected dataset (*yellow*). (**d**) Occipital projections of the corpus callosum. Artifactual parietal fibers connect the two hemispheres due to a vibration artifact (*red*), whereas this is not the case when the artifact is corrected (*yellow*)

References

1. Heemskerk AM, Leemans A, Plaisier A, Pieterman K, Lequin MH, Dudink J. Acquisition guidelines and quality assessment tools for analyzing neonatal diffusion tensor MRI data. AJNR Am J Neuroradiol. 2013;34(8):1496–505.
2. Rohde GK, Barnett AS, Basser PJ, Marenco S, Pierpaoli C. Comprehensive approach for correction of motion and distortion in diffusion-weighted MRI. Magn Reson Med. 2004;51(1):103–14.
3. Tournier JD, Mori S, Leemans A. Diffusion tensor imaging and beyond. Magn Reson Med. 2011;65(6):1532–56.
4. Reese TG, Heid O, Weisskoff RM, Wedeen VJ. Reduction of eddy-current-induced distortion in diffusion MRI using a twice-refocused spin echo. Magn Reson Med. 2003;49(1):177–82.
5. Pajevic S, Pierpaoli C. Color schemes to represent the orientation of anisotropic tissues from diffusion tensor data: application to white matter fiber tract mapping in the human brain. Magn Reson Med. 1999;42(3):526–40.
6. Haselgrove JC, Moore JR. Correction for distortion of echo-planar images used to calculate the apparent diffusion coefficient. Magn Reson Med. 1996;36(6):960–4.
7. Andersson JL, Skare S. A model-based method for retrospective correction of geometric distortions in diffusion-weighted EPI. Neuroimage. 2002;16(1):177–99.
8. Pipe JG. Motion correction with PROPELLER MRI: application to head motion and free-breathing cardiac imaging. Magn Reson Med. 1999;42(5):963–9.
9. Zaitsev M, Dold C, Sakas G, Hennig J, Speck O. Magnetic resonance imaging of freely moving objects: prospective real-time motion correction using an external optical motion tracking system. Neuroimage. 2006;31(3):1038–50.
10. Aksoy M, Forman C, Straka M, Skare S, Holdsworth S, Hornegger J, et al. Real-time optical motion correction for diffusion tensor imaging. Magn Reson Med. 2011;66(2):366–78.
11. Maclaren J, Armstrong BS, Barrows RT, Danishad KA, Ernst T, Foster CL, et al. Measurement and correction of microscopic head motion during magnetic resonance imaging of the brain. PLoS One. 2012;7(11):e48088.

12. Maclaren J, Herbst M, Speck O, Zaitsev M. Prospective motion correction in brain imaging: a review. Magn Reson Med. 2013;69(3):621–36.
13. Leemans A, Jones DK. The B-matrix must be rotated when correcting for subject motion in DTI data. Magn Reson Med. 2009;61(6):1336–49.
14. Gallichan D, Scholz J, Bartsch A, Behrens TE, Robson MD, Miller KL. Addressing a systematic vibration artifact in diffusion-weighted MRI. Hum Brain Mapp. 2010;31(2):193–202.
15. Hiltunen J, Hari R, Jousmaki V, Muller K, Sepponen R, Joensuu R. Quantification of mechanical vibration during diffusion tensor imaging at 3 T. Neuroimage. 2006;32(1):93–103.
16. Greitz D, Wirestam R, Franck A, Nordell B, Thomsen C, Stahlberg F. Pulsatile brain movement and associated hydrodynamics studied by magnetic resonance phase imaging. The Monro-Kellie doctrine revisited. Neuroradiology. 1992;34(5):370–80.
17. Jones DK, Pierpaoli C. Contribution of cardiac pulsation to variability of tractography results. 2005. p. 222.
18. Pierpaoli C, Marenco S, Rohde G, Jones DK, Barnett AS. Analyzing the contribution of cardiac pulsation to the variability of quantities derived from the diffusion tensor. 2003. p. 70.
19. Le Bihan D, Turner R. Intravoxel incoherent motion imaging using spin echoes. Magn Reson Med. 2005;19(2):221–7.
20. Holdsworth SJ, Skare S, Newbould RD, Guzmann R, Blevins NH, Bammer R. Readout-segmented EPI for rapid high resolution diffusion imaging at 3 T. Eur J Radiol. 2008;65(1):36–46.
21. Skare S, Andersson JL. On the effects of gating in diffusion imaging of the brain using single shot EPI. Magn Reson Imaging. 2001;19(8):1125–8.
22. Wirestam R, Greitz D, Thomsen C, Brockstedt S, Olsson MB, Stahlberg F. Theoretical and experimental evaluation of phase-dispersion effects caused by brain motion in diffusion and perfusion MR imaging. J Magn Reson Imaging. 1996;6(2):348–55.
23. Nunes RG, Jezzard P, Clare S. Investigations on the efficiency of cardiac-gated methods for the acquisition of diffusion-weighted images. J Magn Reson. 2005;177(1):102–10.
24. Chang LC, Jones DK, Pierpaoli C. RESTORE: robust estimation of tensors by outlier rejection. Magn Reson Med. 2005;53(5):1088–95.
25. Tax CMW, Otte WM, Viergever MA, Dijkhuizen RM, Leemans A. REKINDLE: robust extraction of kurtosis INDices with linear estimation. Magn Reson Med. 2015;73(2):794–808.
26. Farzaneh F, Riederer SJ, Pelc NJ. Analysis of T2 limitations and off-resonance effects on spatial resolution and artifacts in echo-planar imaging. Magn Reson Med. 1990;14(1):123–39.
27. Skare S, Newbould RD, Clayton DB, Bammer R. Propeller EPI in the other direction. Magn Reson Med. 2006;55(6):1298–307.
28. Romeo F, Hoult DI. Magnet field profiling: analysis and correcting coil design. Magn Reson Med. 1984; 1(1):44–65.
29. Gruetter R. Automatic, localized in vivo adjustment of all first- and second-order shim coils. Magn Reson Med. 1993;29(6):804–11.
30. Sodickson DK, Manning WJ. Simultaneous acquisition of spatial harmonics (SMASH): fast imaging with radiofrequency coil arrays. Magn Reson Med. 1997;38(4):591–603.
31. Pruessmann KP, Weiger M, Scheidegger MB, Boesiger P. SENSE: sensitivity encoding for fast MRI. Magn Reson Med. 1999;42(5):952–62.
32. Griswold MA, Jakob PM, Heidemann RM, Nittka M, Jellus V, Wang J, et al. Generalized autocalibrating partially parallel acquisitions (GRAPPA). Magn Reson Med. 2002;47(6):1202–10.
33. Engstrom M, Bammer R, Skare S. Diffusion weighted vertical gradient and spin echo. Magn Reson Med. 2012;68(6):1755–63.
34. Holdsworth SJ, Yeom K, Skare S, Gentles AJ, Barnes PD, Bammer R. Clinical application of readout-segmented- echo-planar imaging for diffusion-weighted imaging in pediatric brain. AJNR Am J Neuroradiol. 2011;32(7):1274–9.
35. Jezzard P, Balaban RS. Correction for geometric distortion in echo planar images from B0 field variations. Magn Reson Med. 1995;34(1):65–73.
36. Jones DK, Cercignani M. Twenty-five pitfalls in the analysis of diffusion MRI data. NMR Biomed. 2010; 23(7):803–20.
37. Chang H, Fitzpatrick JM. A technique for accurate magnetic resonance imaging in the presence of field inhomogeneities. IEEE Trans Med Imaging. 1992; 11(3):319–29.
38. Irfanoglu MO, Walker L, Sarlls J, Marenco S, Pierpaoli C. Effects of image distortions originating from susceptibility variations and concomitant fields on diffusion MRI tractography results. Neuroimage. 2012; 61(1):275–88.
39. Buonocore MH, Gao L. Ghost artifact reduction for echo planar imaging using image phase correction. Magn Reson Med. 1997;38(1):89–100.
40. Hu X, Le TH. Artifact reduction in EPI with phase-encoded reference scan. Magn Reson Med. 1996; 36(1):166–71.
41. Zhang Y, Wehrli FW. Reference-scan-free method for automated correction of Nyquist ghost artifacts in echoplanar brain images. Magn Reson Med. 2004; 51(3):621–4.
42. Haacke EM, Brown RW, Thompson MR, Venkatesan R. Magnetic resonance imaging: physical principles and sequence design. 82nd ed. New York, NY: Wiley-Liss; 1999.
43. Sarra SA. Digital total variation filtering as post-processing for Chebyshev pseudospectral methods for conservation laws. Numer Algorithm. 2006;41(1): 17–33.

44. Archibald R, Gelb A. A method to reduce the Gibbs ringing artifact in MRI scans while keeping tissue boundary integrity. IEEE Trans Med Imaging. 2002; 21(4):305–19.
45. Bakir T, Reeves SJ. A filter design method for minimizing ringing in a region of interest in MR spectroscopic images. IEEE Trans Med Imaging. 2000;19(6): 585–600.
46. Perrone D, Aelterman J, Pižurica A, Jeurissen B, Philips W, Leemans A. The effect of Gibbs ringing artifacts on measures derived from diffusion MRI. Neuroimage. 2015;120:441–55. http://www.ncbi.nlm.nih.gov/pubmed/26142273.
47. Veraart J, Fieremans E, Jelescu IO, Knoll F, Novikov DS. Gibbs ringing in diffusion MRI. Magn Reson Med. 2015. Forthcoming. http://www.ncbi.nlm.nih.gov/pubmed/26257388
48. Le Bihan D, Poupon C, Amadon A, Lethimonnier F. Artifacts and pitfalls in diffusion MRI. J Magn Reson Imaging. 2006;24(3):478–88.
49. Meyer CH, Pauly JM, Macovski A, Nishimura DG. Simultaneous spatial and spectral selective excitation. Magn Reson Med. 1990;15(2):287–304.
50. Kaldoudi E, Williams SC, Barker GJ, Tofts PS. A chemical shift selective inversion recovery sequence for fat-suppressed MRI: theory and experimental validation. Magn Reson Imaging. 1993;11(3):341–55.
51. Haase A, Frahm J, Hanicke W, Matthaei D. 1H NMR chemical shift selective (CHESS) imaging. Phys Med Biol. 1985;30(4):341–4.
52. Gomori JM, Holland GA, Grossman RI, Gefter WB, Lenkinski RE. Fat suppression by section-select gradient reversal on spin-echo MR imaging. Work in progress. Radiology. 1988;168(2):493–5.
53. Nagy Z, Weiskopf N. Efficient fat suppression by slice-selection gradient reversal in twice-refocused diffusion encoding. Magn Reson Med. 2008;60(5):1256–60.
54. Sarlls JE, Pierpaoli C, Talagala SL, Luh WM. Robust fat suppression at 3T in high-resolution diffusion-weighted single-shot echo-planar imaging of human brain. Magn Reson Med. 2011;66(6):1658–65.
55. De Santis S, Evans CJ, Jones DK. RAPID: a routine assurance pipeline for imaging of diffusion. Magn Reson Med. 2012;70(2):490–6.
56. Walker L, Curry M, Nayak A, Lange N, Pierpaoli C. A framework for the analysis of phantom data in multicenter diffusion tensor imaging studies. Hum Brain Mapp. 2012;34(10):2439–54.
57. Teipel SJ, Reuter S, Stieltjes B, Acosta-Cabronero J, Ernemann U, Fellgiebel A, et al. Multicenter stability of diffusion tensor imaging measures: a European clinical and physical phantom study. Psychiatry Res. 2011;194(3):363–71.
58. Pullens P, Roebroeck A, Goebel R. Ground truth hardware phantoms for validation of diffusion-weighted MRI applications. J Magn Reson Imaging. 2010;32(2): 482–8.
59. Fillard P, Descoteaux M, Goh A, Gouttard S, Jeurissen B, Malcolm J, et al. Quantitative evaluation of 10 tractography algorithms on a realistic diffusion MR phantom. Neuroimage. 2011;56(1):220–34.
60. Boujraf S, Luypaert R, Eisendrath H, Osteaux M. Echo planar magnetic resonance imaging of anisotropic diffusion in asparagus stems. MAGMA. 2001;13(2): 82–90.
61. Campbell JS, Siddiqi K, Rymar VV, Sadikot AF, Pike GB. Flow-based fiber tracking with diffusion tensor and q-ball data: validation and comparison to principal diffusion direction techniques. Neuroimage. 2005; 27(4):725–36.
62. Beaulieu C. The basis of anisotropic water diffusion in the nervous system: a technical review. NMR Biomed. 2002;15(7–8):435–55.
63. Lin CP, Wedeen VJ, Chen JH, Yao C, Tseng WY. Validation of diffusion spectrum magnetic resonance imaging with manganese-enhanced rat optic tracts and ex vivo phantoms. Neuroimage. 2003;19(3): 482–95.
64. Lorenz R, Bellemann ME, Hennig J, Il'yasov KA. Anisotropic phantoms for quantitative diffusion tensor imaging and fiber-tracking validation. Appl Magn Reson. 2008;33(4):419–29.
65. White T, Nelson M, Lim KO. Diffusion tensor imaging in psychiatric disorders. Top Magn Reson Imaging. 2008;19(2):97–109.
66. Andersson JL, Richter M, Richter W, Skare S, Nunes RG, Robson MD, et al. Effects of susceptibility distortions on tractography. Kyoto: ISMRM; 2004.

Suggested Reading

67. Andersson JLR, Skare S. Image distortion and its correction in diffusion MRI. In: Jones DK, editor. Diffusion MRI: theory, methods, and applications. New York, NY: Oxford University Press; 2010.
68. Pierpaoli C. Artifacts in diffusion MRI. In: Jones DK, editor. Diffusion MRI: theory, methods, and applications. New York, NY: Oxford University Press; 2010.